Rare Metal Materials and Engineering
Volume 54, Issue 8, August 2025
Available online at www.rmme.ac.cn

Science Press

Cite this article as: Li Yuli, Chen Qiuyu, Li Hao, et al. Effect of Hydrogen Content on Static and Dynamic Mechanical Behavior of Zr-Sn-Nb-Fe Alloy[J]. Rare Metal Materials and Engineering, 2025, 54(08): 1956-1961. DOI: https://doi.org/10.12442/j.issn.1002-185X.20240430.

ARTICLE

Effect of Hydrogen Content on Static and Dynamic Mechanical Behavior of Zr-Sn-Nb-Fe Alloy

Li Yuli, Chen Qiuyu, Li Hao, Sun Taotao, Qu Jingwen, Liu Qiong

Xi'an Western Energy Material Technologies Co., Ltd, Xi'an 710016, China

Abstract: Zirconium alloy cladding materials inevitably undergo hydrogen absorption in the processing and operation process of the reactor, and its static and dynamic mechanical properties are closely related to the hydrogen content. Samples with hydrogen content ranging from 23 μg/g to 132 μg/g were obtained using the method of gas-phase hydrogen charging, and the influence of hydrogen content on static/dynamic mechanical properties of Zr-Sn-Nb-Fe alloy was studied. The results show that the effect of weak hydrogen charging on the ultimate tensile strength, yield strength, and elongation of zirconium alloy is not obvious. There are a large number of dimples on the fracture surface of the tensile sample before and after hydrogen charging, which is a typical ductile fracture. However, the impact toughness of Zr-Sn-Nb-Fe alloy decreases significantly after trace hydrogen charging. The impact sample without hydrogen charging shows the mixed fracture mechanism of ductile fracture and microcleavage fracture. The increase in hydrogen permeability leads to the emergence of hydride, and the deformation of high strain rate under the impact loading condition leads to secondary cracks in the microstructure. The initiation and expansion of the secondary cracks is the main reason for the reduction of the impact toughness.

Key words: Zr-Sn-Nb-Fe; hydrogen content; tensile property; impact property

1 Introduction

As an advanced cladding material for nuclear reactor fuel elements, Zr-Sn-Nb-Fe alloy has the advantages of low neutron absorption cross section, good corrosion resistance, high mechanical strength, and stable size under irradiation[1]. During the alloy processing or reactor operation, zirconium alloy cladding tube will inevitably absorb hydrogen. Due to the extremely low solid solubility of hydrogen in zirconium, most hydrogen precipitates in the form of hydrides[2–4]. According to the influence of hydride on the mechanical properties of zirconium alloy, existing studies[5–7] indicate that hydride has intrinsic fragility, which can decrease ductility and lead to deformation cracking of zirconium alloy. For example, research of hydrogen charging in zirconium alloy[8–11] has shown that when the hydrogen content exceeds 500 μg/g, the disorder distribution of hydride will deteriorate the tensile performance of zirconium alloy.

Therefore, despite extensive research on the influence of hydride on the mechanical properties of zirconium alloys, the influence of trace hydrogen content on the mechanical properties of zirconium alloys remains underexplored. Unlike quasi-static stretching process, industrial manufacturing techniques such as high-speed rolling, punching, and high-speed cutting involve the high-strain rate deformation under the impact loading condition. Current studies have paid limited attention to the dynamic mechanical properties of zirconium alloy. This study investigated the effects of different hydrogen contents on the static and dynamic mechanical properties of Zr-Sn-Nb-Fe alloys through quasi-static tensile testing, pendulum impact testing, and post-fracture morphology and properties analyses. The results are of great significance for the production and safe service of zirconium alloy fuel cladding.

2 Experiment

The experimental samples were Zr-Sn-Nb-Fe alloy tube billets in the recrystallization state, which were processed

Received date: July 16, 2024
Foundation item: CNNC Youth Talent Program (CNNC-SFTYS-202201)
Corresponding author: Chen Qiuyu, Ph. D., Xi'an Western Energy Material Technologies Co., Ltd, Xi'an 710016, P. R. China, Tel: 0086-29-86066030, E-mail: 303532250@qq.com

through melting, quenching, hot extrusion, cold rolling, and annealing. Their nominal composition was Zr-1.0Sn-1.0Nb-0.1Fe (wt%). The gas-phase hydrogen charging of the as-prepared intact samples was carried out in an atmosphere tube furnace using a mixed gas atmosphere consisting of hydrogen (2vol%) and argon (98vol%). Samples with different contents of hydrogen were obtained by varying the gas flow rate and holding time, as listed in Table 1.

The samples were cut into the dimensions of Φ21 mm×100 mm and 55 mm×10 mm×10 mm samples using the electric spark cutting machine (STX-202A, China). After acetone cleaning, ultrasonic cleaning, pure water cleaning, alcohol cleaning, and low-temperature drying treatments, the samples were put into an atmospheric tube furnace. The mixed gas should be pre-connected for about 15 min before the test, and then the furnace was heated to 400 °C with holding time of 10, 20, 40, and 60 min. The hydrogen content in the samples was determined by an H836hydrogen analyzer (LECO, American).

The macroscopic fracture morphology of the samples was observed using a 3D superfield depth microscope (OLYMPUS DSX10-UZH, Japan). The microscopic morphology of the sample and the fracture morphology were observed using a Hitachi SU6600 thermal field emission scanning electron microscope, with an accelerating voltage of 15 kV.

The room-temperature tensile tests of the alloy were carried out on testing machine (Instron 5565, America). All performance tests were repeated three times to ensure the reliability and accuracy of the results. The displacement-controlled tensile tests at the tensile rate of 5×10^{-4} mm/min were conducted at room temperature. The tensile sample dimensions are shown in Fig.1.

Impact test was carried out for the received samples through a Charpy impact test machine at room temperature. The size of the impact sample is shown in Fig.2. V-notch type impact samples were used in this research for comprehensively evaluating the entire fracture process, including crack initiation, and fitting the actual impact toughness of alloy. Impact energy presented in this study was an average of three values obtained from the samples with different processing parameters. The maximum shock absorption energy of the test machine was 15 J at room temperature.

Table 1 Gas- pahse hydrogen charging conditions and hydrogen content of samples

Sample	Gas flow rate/L·h^{-1}	Holding time/min	Hydrogen content/μg·g^{-1}
1#	0	0	3
2#	40	10	23
3#	40	20	38
4#	40	40	89
5#	40	60	132

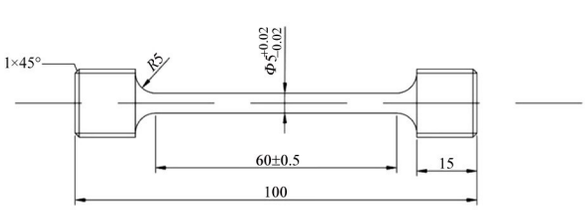

Fig.1 Dimension of samples for tensile tests

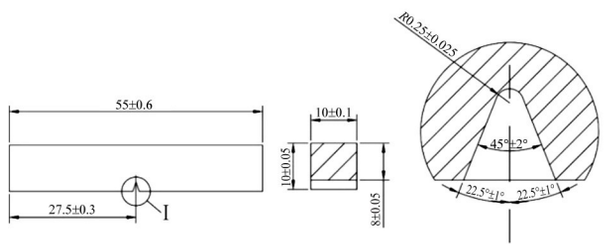

Fig.2 Dimension of samples for impact tests

3 Results and Discussion

3.1 Tensile performance and fracture morphology

Quasi-static room-temperature tensile tests were conducted on Zr-Sn-Nb-Fe alloy samples with different hydrogen contents, and the stress-strain curves are shown in Fig. 3. The stress-strain curves for samples before and after hydrogen charging are similar, exhibiting three distinct stages: elastic deformation, plastic deformation, and uneven deformation, consistent with the characteristics of toughness fracture. When the stress-strain curve is in elastic deformation stage, the stress is directly proportional to the strain. When the load exceeds the yield strength (YS), the sample undergoes dispersion instability: the stress increases extremely slowly in a short period as the pores appear inside the matrix. Finally, the sample shrinks and finally fractures when the load reaches the peak. The detailed tensile performance results are summarized in Table 2. The ultimate tensile strength (UTS) of Zr-Sn-Nb-Fe samples before hydrogen charging can reach 551 MPa. When the hydrogen content reaches 132 μg/g, UTS of Zr-Sn-Nb-Fe sample reaches 543 MPa. The results show that the UTS, YS, and elongation of Zr-Sn-Nb-Fe alloy show no significant dependence on hydrogen content.

Quasi-static tensile fracture morphologies of Zr-Sn-Nb-Fe alloy with different hydrogen contents are shown in Fig. 4. Without hydrogen charging, the tensile fracture surface is rough and continuous, with a large number of dimples, indicating a typical ductile fracture. Further observations of the tensile fracture morphology of Zr-Sn-Nb-Fe alloy with hydrogen content of 23 μg/g show that no obvious cracks and large size holes are found. It is due to the hole left by the detachment of the second phase from the matrix under tensile stress. When the hydrogen content increases to 89 μg/g, trace cracks appear in the tensile fracture port, with a crack length of about 10 μm. With the continuous increase in hydrogen content to 132 μg/g, the tensile fracture of Zr-Sn-Nb-Fe sample is still a ductile fracture, but the size of dimples increases and their number decreases. At the same time, the

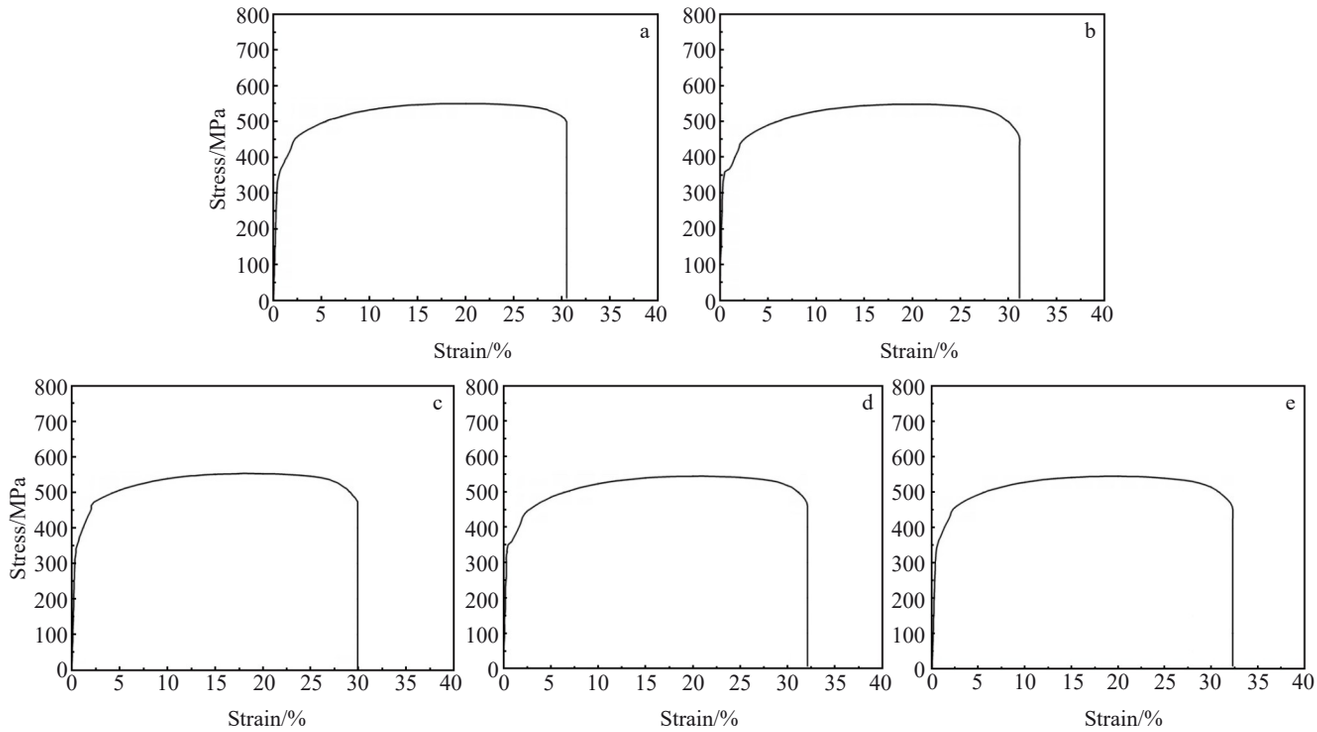

Fig.3 Stress-strain curves of different samples: (a) 1#, (b) 2#, (c) 3#, (d) 4#, and (e) 5#

Table 2 Tensile results of samples with different hydrogen contents

Sample	UTS/MPa	YS/MPa	Elongation/%
1#	551	353	23.4
2#	548	359	23.6
3#	550	350	23.6
4#	544	349	24.2
5#	543	343	23.9

number of cracks in the fracture increases. However, the effect on tensile strength is not obvious.

When the hydride-induced cracks deform at relatively low strain rates, the shape and size of the cracks will expand with the tensile deformation process. Hence, some cracks may disappear in the plastic deformation stage. Moreover, due to the excellent matrix toughness of Zr-Sn-Nb-Fe alloy, the hydride formed by trace hydrogen charging is less and not reunited, and the crack tip exhibits passivation behavior at low strain rate, which greatly delays the crack extension. Therefore, the increase in hydrogen content does not significantly affect the tensile strength of Zr-Sn-Nb-Fe alloy.

3.2 Impact toughness and fracture morphology

Charpy impact tests combined with microstructure observations were performed on Zr-Sn-Nb-Fe alloy with different hydrogen contents. As can be seen from Table 3, the impact toughness changes significantly before and after hydrogen charging. The impact strength of Zr-Sn-Nb-Fe sample before hydrogen charging is 37.4 J/cm^2. When the hydrogen content increases to just 23 μg/g, the impact toughness rapidly drops to 30.3 J/cm^2; further increasing the hydrogen content to 132 μg/g reduces the impact toughness to only 19.4 J/cm^2. The substantial decrease in impact toughness of Zr-Sn-Nb-Fe alloy observed in Table 3 can be attributed to the changes in the internal structure of the alloy. Consequently, subsequent characterization of the dynamic impact fracture morphology of Zr-Sn-Nb-Fe alloys with different hydrogen contents is necessary to elucidate this phenomenon.

The fracture morphology of samples after the impact test is generally divided into three parts: fiber area, radiation area, and shear lip. Fig. 5a is the macro morphology of the impact fracture of sample before hydrogen charging. As can be seen, the morphology is flat, with plastic acute deformation at the edges. The shear area, fiber area, and radiation area can be distinguished at the fracture morphology. Microscopic analysis reveals a large number of dimples in the impact fracture of Zr-Sn-Nb-Fe alloy, along with minor river-like brittle fracture features and a few micropores. This indicates a predominantly ductile fracture mechanism with mixed microcleavage fracture mechanism. With the increase in hydrogen content, the fiber area at the fracture decreases, while the radiation area becomes dominant. The increase in micropore in the fracture and the hole combination leads to the occurrence of cracks under the load. When the hydrogen content reaches 132 μg/g, the macro morphology of the impact fracture, as shown in Fig. 5b, shows obvious relief at the center of the impact fracture. It is found that the fracture area has almost no fiber area, consisting almost entirely of the radial area. Further microscopic analysis of the microscopic

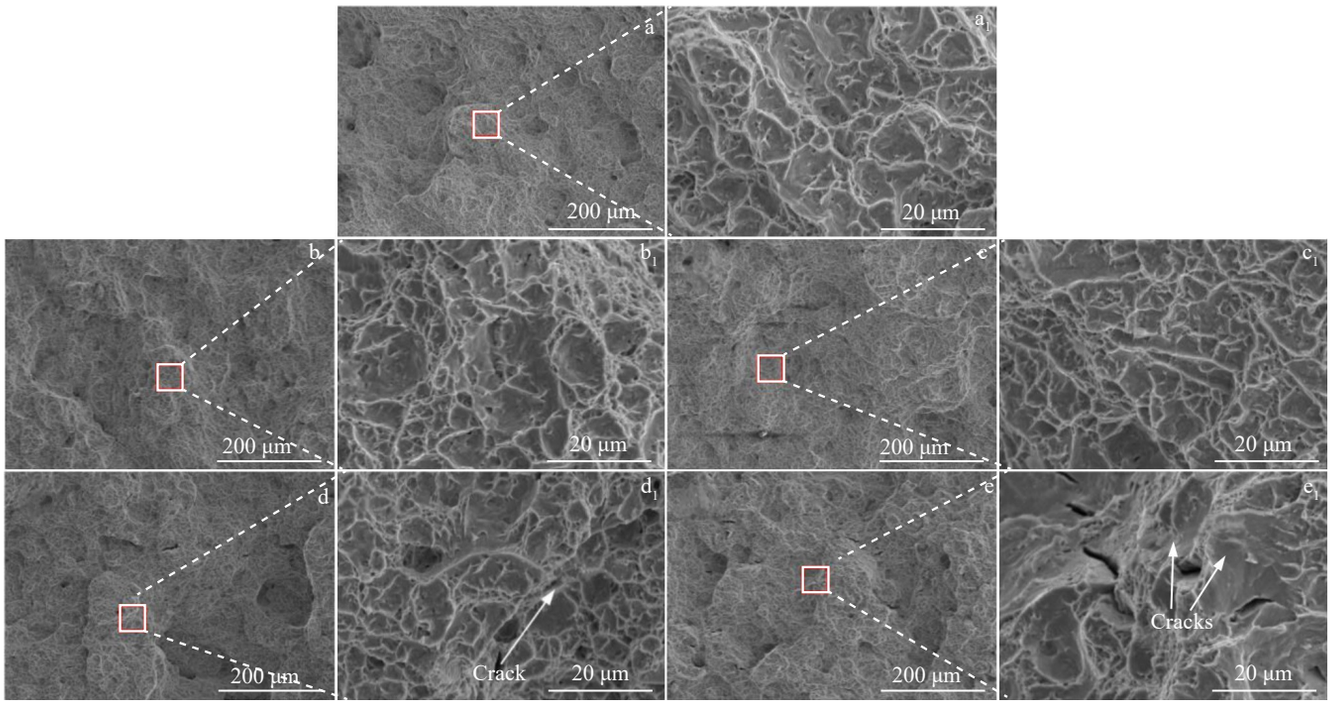

Fig.4 Tensile fracture morphologies of samples with different hydrogen contents: (a, a_1) 1#, (b, b_1) 2#, (c, c_1) 3#, (d, d_1) 4#, and (e, e_1) 5#

Table 3 Impact test results of samples with different hydrogen contents

Sample	Impact absorbing energy/J	Impact toughness/ J·cm^{-2}
1#	22.5	37.4
2#	18.3	30.3
3#	16.4	27.2
4#	13.7	22.7
5#	11.7	19.4

morphology (Fig. 6d) reveals a lot of cracks up to 50 μm in length in the fracture, exhibiting no obvious directional preference. Although there are still a large number of dimples in the impact fracture, the fracture interface is clear at the crack, and the fracture line is smooth and straight, showing obvious brittle fracture characteristics. This indicates that the fracture morphology presents a mixed ductile-cleavage fracture mechanism. The hydrogen charging leads to the formation of hydride, and the high-strain rate deformation under impact loading conditions induces secondary crack in the microstructure structure of Zr-Sn-Nb-Fe alloy. The initiation and expansion of these secondary cracks are the main reason for the reduction of impact toughness.

3.3 Tensile properties and impact properties

Through the analysis of the tensile and impact properties of Zr-Sn-Nb-Fe alloy with different hydrogen contents, it is found that trace hydrogen has little influence on the tensile properties and fracture morphology of the sample, but it has a significant impact on the impact toughness. Generally speaking, the static tensile process involves a low deformation strain rate compared to the dynamic impact

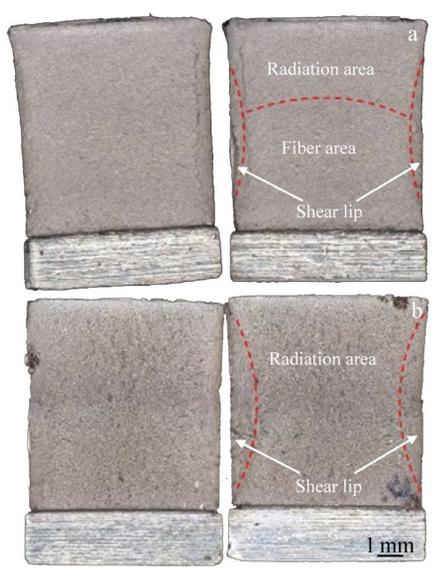

Fig.5 Macros morphologies of impact samples 1# (a) and 5# (b)

process (tensile strain rate: 5×10^{-4} s^{-1}; impact strain rate: $10^{2}-10^{-4}$ s^{-1}) [12]. The micropores and cracks in the deformation are prone to passivation under the low-strain rate deformation conditions, which greatly delays the crack extension, thus without excessive influence on the tensile strength of the alloy. The dynamic impact testing evaluates the crack expansion under high-strain rates deformation conditions. The brittle hydride appears in the microstructure of Zr-Sn-Nb-Fe alloy after hydrogen charging, providing preferential pathways for crack initiation and propagation with minimal resistance, and thereby leading to the reduction of the impact power[13].

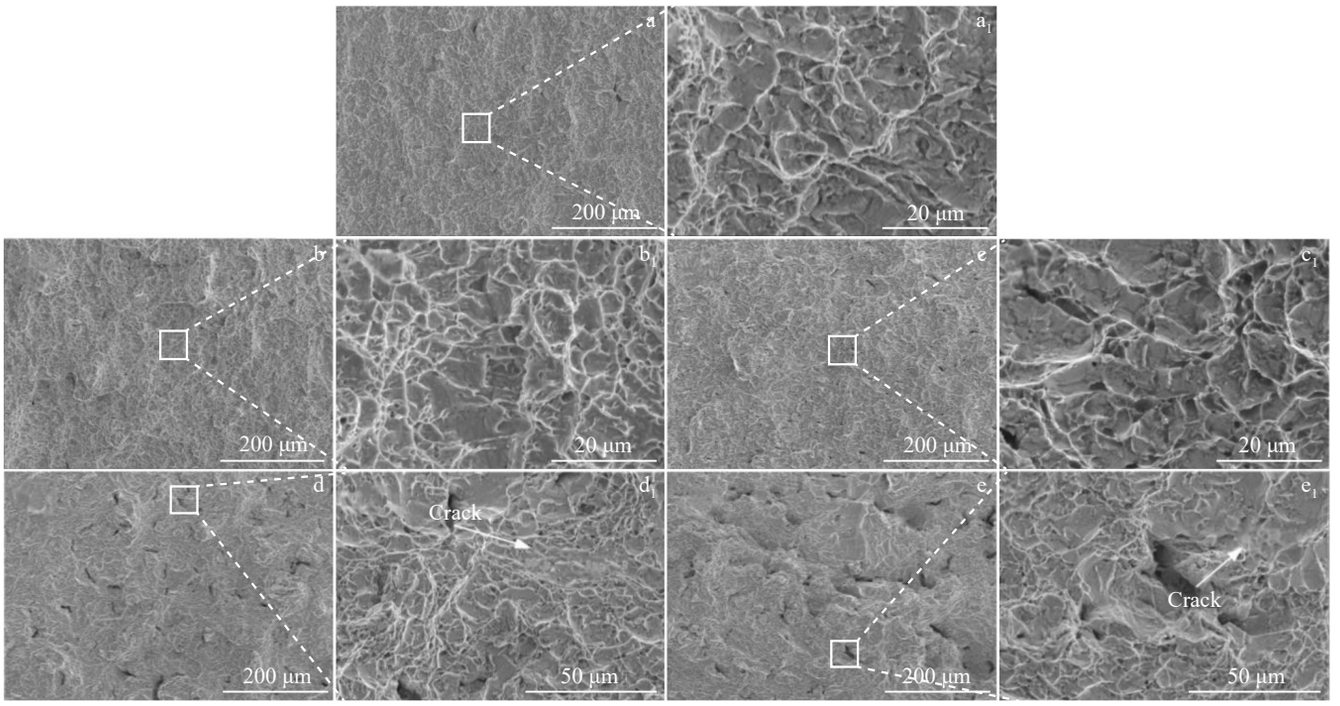

Fig.6 Impact fracture morphology of samples with different hydrogen contents: (a, a_1) 1#, (b, b_1) 2#, (c, c_1) 3#, (d, d_1) 4#, and (e, e_1) 5#

To better explain the load transfer mechanisms in zirconium alloys and the associated microstructural changes, the tensile fracture process of Zr-Sn-Nb-Fe alloy after hydrogen charging is described in Fig.7.

For Zr-Sn-Nb-Fe alloy after hydrogen charging, the tensile fracture process exhibits three stages[14–15]. (1) Under the action of tensile stress, the grain of the matrix is elongated through the boundary migration, and the fine second phases with will migrate toward the grain boundaries. (2) With continuous stress, cross-sectional necking occurs, accompanied by void formation at the interface of hydride and matrix. (3) The zirconium matrix undergoes ductile fracture under load. At high strain rate, the ride near the V-notch is subjected to tensile stress, while the opposite side undergoes compressive stress. Upon impact, the internal holes lack sufficient time to deform; crack is initiated and propagated along the hydride phases, finally leading to instantaneous fracture.

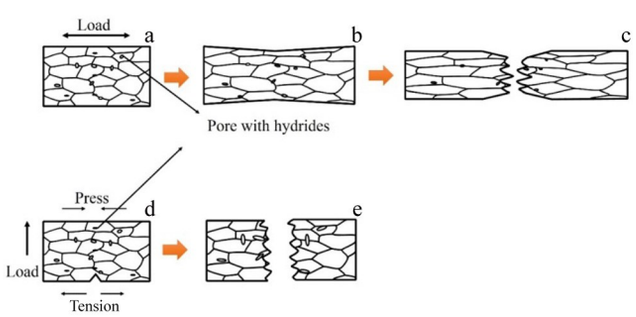

Fig.7 Schematics of tensile fracture (a–c) and impact fracture (d–e) processes of Zr-Sn-Nb-Fe alloy: (a, d) loading stage, (b) neck reduction stage, and (c, e) fracture stage

4 Conclusions

1) At room temperature, with the increase in hydrogen content from 3 μg/g to 132 μg/g, the UTS, YS, and elongation of Zr-Sn-Nb-Fe alloy exhibit no obvious fluctuations. Quasi-static tensile fracture morphology characterization of Zr-Sn-Nb-Fe alloy with different hydrogen contents reveals that both the samples before and after hydrogen charging display numerous ductile dimples on their fracture surfaces, which is a typical of ductile fracture behavior.

2) The impact toughness of Zr-Sn-Nb-Fe alloy before hydrogen charging is 37.4 J/cm^2, and it decreases significantly with the increase in hydrogen content. Characterization of the dynamic impact fracture morphology of samples with different hydrogen contents reveals that the fracture mechanism of sample before hydrogen charging is basically ductile fracture with a mixed microcleavage fracture. With the increase in hydrogen content, hydrides form, and the high-strain rate deformation under impact loading conditions leads to secondary cracks in the microstructure of Zr-Sn-Nb-Fe alloy. The initiation and propagation of secondary cracks are the main reasons for the decrease in impact toughness.

3) Hydrogen absorption is inevitable during the deformation processing and service of zirconium alloy. Industrial production processes such as high-speed rolling, punching, and high-speed cutting involve high-strain rate deformation under impact loading conditions. Current research has predominantly focused on the influence of hydrides on the tensile performance of the alloy, with limited attention to their behavior under dynamic impact conditions. Exploring the

evolution of hydride and secondary cracks in the process of dynamic impact will play a guiding role in the subsequent processing and service process of zirconium alloy.

References

1 Xu Chunrong, Zhao Wenjin, Xie Meng *et al*. *Rare Metal Materials and Engineering*[J], 2017, 46(12): 3922

2 Bai J B, Prioul C, Lansiart S *et al*. *Scripta Metallurgica et Materialia*[J], 1991, 25: 2559

3 Xiao Lin, Yukichi Umakoshi, Sun Jun. *Materials Science & Engineering A*[J], 2000, 292(1): 40

4 Ding Xiangdong, Wang Ruihong, Liu Gang *et al*. *Acta Materialia*[J], 2003, 39(3): 267

5 Thai Le Hong, Jean-Christophe Brachet, Jérôme Crépin *et al*. *Journal of Nuclear Materials*[J], 2021, 554: 153069

6 Liu Jinyun, Pu Xia, Sun Chao *et al*. *Rare Metal Materials and Engineering*[J], 2017, 46(3): 711

7 Kim Sangbum, Kang Joo-Hee, Lee Youho. *Journal of Nuclear Materials*[J], 2022, 559: 153393

8 Zhang Yin, Song Xiping. *Materials Science & Engineering A*[J], 2021, 811: 141093

9 Sun Huanzheng, Luan Baifeng, Zhu Xiaoyang *et al*. *Materials Characterization*[J], 2022, 194: 112396

10 Kim Ju-Seong, Kim Tae-Hoon, Kook Dong-Hak *et al*. *Journal of Nuclear Materials*[J], 2015, 456: 235

11 Zhou Bangxin, Yao Meiyi. *Nuclear Reactor Materials*[M]. Shanghai: Shanghai Jiao Tong University Press, 2021: 125 (in Chinese)

12 Brendan Ensor. *Journal of Nuclear Materials*[J], 2023, 574: 154149

13 Li Yao, Gao Huixian, Li Qinqin *et al*. *Weapon Materials and Mechanics*[J], 1984, 6: 3

14 Chen Qiuyu, Liang Shuhua, Zhang Xiaochuan *et al*. *Journal of Alloys and Compounds*[J], 2021, 886: 161286

15 Cui Kaixuan, Qiao Junwe, Liaw Peter K *et al*. *Science China Physics, Mechanics & Astronomy*[J], 2024, 67: 227101

氢含量对Zr-Sn-Nb-Fe合金静动态力学性能的影响

李宇力，陈秋羽，李　豪，孙涛涛，渠静雯，刘　琼

(西安西部新锆科技股份有限公司，陕西 西安 710016)

摘　要：锆合金包壳材料在加工过程及反应堆内运行过程中都不可避免会发生吸氢，而其静动态力学性能的变化与氢含量有着密切的联系。采用气相渗氢的方法，获得了氢含量在23~132 μg/g范围的试样，研究了氢含量对Zr-Sn-Nb-Fe合金静动态力学性能的影响。结果表明，微量渗氢后的锆合金极限抗拉伸强度、屈服强度及延伸率的变化并不明显。渗氢前后的拉伸试样表面存在大量韧窝，是典型的韧性断口。而微量渗氢后的Zr-Sn-Nb-Fe合金冲击韧性出现大幅下降。未渗氢的冲击样品断口基本呈现韧性断裂为主，结合微量解理断裂的混合断裂机制。随着渗氢量的增加，氢化物出现。冲击加载条件下的高应变速率变形则会导致合金微观组织结构中出现二次裂纹，二次裂纹的萌生及扩展是冲击韧性降低的主要原因。

关键词：Zr-Sn-Nb-Fe；氢含量；拉伸性能；冲击性能

作者简介：李宇力，男，1987年生，博士，高级工程师，西安西部新锆科技股份有限公司，陕西 西安 710016，Tel：029-86066030，E-mail：15503511186@163.com